Modeling the properties of ferrogels in uniform magnetic fields

Dean S. Wood and Philip J. Camp*

School of Chemistry, The University of Edinburgh, West Mains Road, Edinburgh EH9 3JJ, United Kingdom

(Received 2 August 2010; revised manuscript received 10 November 2010; published 7 January 2011)

The properties of ferrogels in homogeneous magnetic fields are studied using a simple microscopic model and Monte Carlo simulations. The main phenomena of interest concern the anisotropy and enhancement of the elastic moduli that result from applying uniform magnetic fields before and after the magnetic grains are locked in to the polymer-gel matrix by cross-linking reactions. The positional organization of the magnetic grains is influenced by the application of a magnetic field during gel formation, leading to a pronounced anisotropy in the mechanical response of the ferrogel to an applied magnetic field. In particular, the elastic moduli can be enhanced to different degrees depending on the mutual orientation of the fields during and after ferrogel formation. The model represents ferrogels by ensembles of dipolar spheres dispersed in elastic matrices. Experimental trends are shown to be reflected accurately in the simulations of the microscopic model. In addition, the simulations yield microscopic insights on the organization of the magnetic grains. Finally, simple relationships between the elastic moduli and the magnetization are proposed. If supplemented by the magnetization curve, these relationships yield the dependencies of the elastic moduli on the applied magnetic field, which are often measured directly in experiments.

DOI: 10.1103/PhysRevE.83.011402 PACS number(s): 83.80.Kn, 75.80.+q, 61.41.+e, 75.60.Ej

I. INTRODUCTION

A ferrogel is composed of microscopic magnetic grains firmly embedded in an elastic cross-linked polymer gel matrix [1–3]. Grains on the 10-nm scale are usually ferromagnetic or intrinsically superparamagnetic, carrying magnetic dipole moments which can be estimated from the bulk magnetization volume of the constituent magnetic material (usually transition metals or their oxides), while grains on the 100-nm–1-μm scale may possess several randomly oriented magnetic domains [4]. Traditionally, magnetic polymer composites have been fashioned from materials with rather high elastic moduli, meaning that the mechanical responses of the composites to external magnetic fields are insignificant. Ferrogels, on the other hand, are made from polymeric constituents with much lower elastic moduli, leading to enhanced magnetic and mechanical responses to external stimuli. The coupling between magnetic and mechanical properties leads to a large number of functionalities and applications. Ferrogels can be used as soft actuators in which magnetic stimuli (such as magnetic-field gradients) lead to deformations; examples of applications include crawling "robots" [5,6], media for localized hyperthermic treatment [7,8] and drug delivery [9], and artificial muscles [10,11]. Stresses, strains, temperature changes, and chemical stimuli (such as changes in pH and ionic strength or the addition of swelling agents) act primarily on the polymer-gel matrix but lead to changes in the magnetic susceptibility and so a ferrogel may also function as a sensor [12].

Magnetic gels also play key roles in the formation of crack patterns in thin films of magnetic colloidal suspensions drying on a substrate in the presence of a magnetic field [13,14]. As the solvent evaporates and the magnetic grains become more concentrated, the suspension forms a gel phase which then adheres to the substrate. As more solvent evaporates, large tensile stresses build up due to the shrinkage of the thin film and the adhesion of the film to the substrate. At some point, the film ruptures and crack patterns appear. It turns out that the spacings between cracks—whether directional or isotropic—follow a universal scaling law depending on the thickness of the film [13]. In addition, the shapes of cracks can be used to estimate the Young's modulus of the gel just prior to crack formation [14].

The properties of ferrogels are dictated by the coupling of magnetostriction (field-induced deformation leading to a change in magnetic susceptibility), magnetostatics (interactions between magnetic dipoles), and the elastic properties of the polymer-gel matrix. A manifestation of this coupling can be observed in the deformation of a macroscopic ferrogel body in a uniform magnetic field [15–21]. Since a uniform magnetic field exerts no net force on a magnetic dipole, the deformation is driven entirely by an interplay of the aforementioned effects, and the result depends rather sensitively on the geometry of the ferrogel body. Of course, the most dramatic deformations (even on the order of 100%) can be achieved with the application of magnetic-field gradients [1,2,22–24]. Although such deformations can be rationalized from a relatively simple treatment of the magnetic interactions and the elastic extension of the polymer-gel matrix, there are plenty of nontrivial effects such as magnetic and mechanical hysteresis which require more detailed microscopic descriptions [12].

The mechanical properties of ferrogels exhibit subtle but nonetheless important dependencies on applied uniform magnetic fields. Significantly, the nature and extent of these effects can be tuned by altering the synthetic conditions. In recent work, ferrogels have been *synthesized* in uniform magnetic fields. Before the cross-linking reaction is initiated between the polymers, the magnetic grains can diffuse throughout the sample and adopt whichever microstructures and orientations

*Corresponding author: philip.camp@ed.ac.uk

that minimize the free-energy for the fluid phase in the presence of the magnetic field. Uniform fields are well known to promote chainlike positional and orientational correlations between magnetic grains. Subsequently, the cross-linking reaction can be chemically initiated and the polymer gel is formed, locking in the anisotropic positional microstructure of the magnetic grains. This naturally leads to an anisotropy in the elastic properties of the ferrogel since the forces between the magnetic grains will depend on the directions in which stresses and magnetic fields are applied. This has been demonstrated in a number of experimental situations [12,22–27]. In Ref. [27] for example, 10-to-30-wt% suspensions of iron-carbonyl microspheres in cross-linked polymer gel were prepared in applied fields of 400 mT and then subjected to fields in various orientations. It was found that the elastic modulus can be enhanced to varying degrees depending on the orientation of fields during synthesis and measurement. If no field is applied during synthesis, then the elastic modulus of a 30-wt% ferrogel increases from 13 to 15 kPa (15% increase). If the fields during synthesis and measurement are parallel, then the elastic modulus in the field direction increases from 54 to 87 kPa (61% increase), while those in the transverse directions increase from 26 to 35 kPa (35% increase). If the fields during synthesis and measurement are perpendicular, then the elastic modulus in the measurement-field direction increases from 26 to 28 kPa (8% increase), while that in the synthesis-field direction increases from 54 to 60 kPa (11% increase). The increases in elastic moduli are less pronounced with lower concentrations of magnetic material. Qualitatively similar trends are seen for other ferrogels, including those containing much smaller magnetic grains [23]. Clearly, these features are due to the interplay between the elastic properties of the gel, the distribution of the magnetic particles throughout the ferrogel, and the resulting magnetostatic forces between the dipoles and the applied field.

The aim of this work is to establish a working microscopic model of a ferrogel that incorporates the most important features of the positional microstructure and possesses physical properties that are in good agreement with those of real materials. To this end, a ferrogel is modeled as an elastic continuum in which are embedded interacting dipolar spheres. Given this microscopic model, Monte Carlo (MC) computer simulations are performed to generate typical fluid microstructures and to determine the responses of the resulting ferrogel to applied magnetic fields.

In this preliminary study, the model is restricted to monodisperse dipolar spheres, although it is recognized that polydispersity is an unavoidable experimental fact [28,29]; nonetheless, the good agreement with experiment to be demonstrated in what follows shows that this assumption is valid. Another simplifying assumption is that the ferrogel can only undergo affine distortions. This means that shear deformations and irregular shape distortions are not considered. Shear moduli of elastomers with imbedded magnetic particles can be significantly enhanced with magnetic fields [30], but this more complicated situation will be addressed in future work. It is noted that models with explicit representations of the polymer-gel matrix are perhaps better suited to the case of nonaffine distortions [31], albeit with a greater computational cost. The case of ferromagnetic particles is considered because rather a lot is known about their fluid-phase magnetization properties from a theoretical perspective [32,33] and it turns out that this also provides adequate predictions for the model ferrogels. Typically, ferromagnetic particles are limited to the 10-nm size range [4] and although ferrogels are made with such particles [12,23,24], particles on the 100-nm–1-μm scale are sometimes preferred [22,24–27]. Detailed theoretical predictions for the magnetization curves and magnetic susceptibilities of anisotropic ferrogels are lacking [34]. It will be shown that for the current model there exist simple relationships between the elastic moduli and the magnetization, and so if the magnetization curve is known, then so are the dependencies of the elastic moduli on the magnetic-field strength. Finally, an issue related to the preceding points is that the dipole moment of a magnetic grain may reorient by Néel relaxation and/or by Brownian rotation of the particle as a whole [4]. It is assumed here that the dipole moment is free to rotate unhindered by interactions between the gel matrix and the magnetic grain.

This article is organized as follows. The microscopic model and simulation protocol is described in Sec. II and particular attention is paid to the choices of reduced units and appropriate simulation parameters for useful comparisons with experiment. The simulation results are presented in Sec. III with emphases on the magnitude and anisotropy of the elastic moduli and the relationships between the elastic moduli and the magnetization. Section IV concludes the paper with a summary and an outlook on future developments.

II. MODEL AND METHODS

The ferrogel is modeled as a suspension of dipolar hard spheres (DHSs) trapped in an elastic matrix. The simulated region of the ferrogel is assumed to be orthorhombic and its deformations are restricted to be affine; that is, the coordinates of a particle are equal to $\boldsymbol{r} = (L_x s_x, L_y s_y, L_z s_z)$, where L_α are the box lengths (which may fluctuate) and $-\frac{1}{2} \leqslant s_\alpha \leqslant \frac{1}{2}$ are fractional coordinates (which stay constant).

The following protocol was used to prepare samples of a model gel with a prescribed concentration of magnetic grains. Fluid-phase configurations were generated using standard N-P-T MC simulations [35,36] of $N = 250$ DHSs in a cubic simulation cell of volume $V = L^3$ and with a uniform magnetic field $\boldsymbol{H}_\mathrm{f}$ applied; in what follows, the subscript "f" refers to simulations in the fluid phase. The Boltzmann distribution for the fluid is

$$p_\mathrm{f} \propto V^N \exp\left[-\beta\left(U_\mathrm{DHS} + PV - \mu_0 \boldsymbol{H}_\mathrm{f} \cdot \boldsymbol{M}\right)\right], \qquad (1)$$

where $\beta = 1/k_\mathrm{B}T$, $U_\mathrm{DHS} = \sum_{i<j}^{N} u_{ij}$ is the DHS interaction potential energy, and $\boldsymbol{M} = \sum_i^N \boldsymbol{\mu}_i$ is the magnetization. The pair potential for two DHSs with separation vector $\boldsymbol{r}$ and dipole moments $\boldsymbol{\mu}_i$ and $\boldsymbol{\mu}_j$ is

$$u_{ij} = \begin{cases} \infty & r \leqslant \sigma, \\ \dfrac{\mu_0}{4\pi}\left[\dfrac{\boldsymbol{\mu}_i \cdot \boldsymbol{\mu}_j}{r^3} - \dfrac{3(\boldsymbol{\mu}_i \cdot \boldsymbol{r})(\boldsymbol{\mu}_j \cdot \boldsymbol{r})}{r^5}\right] & r > \sigma, \end{cases} \qquad (2)$$

where σ is the hard-sphere diameter. The long-range dipolar interactions were handled using the Ewald summation with conducting boundary conditions [35]. One MC sweep consisted of, on average, N translational or orientational particle

moves and one volume move. The maximum translational and orientational displacement parameters were adjusted to give acceptance rates of 20% and 50%, respectively. Simulation configurations were saved at intervals of 10^4 sweeps. The *N-P-T* runs yielded an average concentration $\rho = \langle N/V \rangle$ and an average fluid box length $\langle L \rangle_f$. At least 20 independent fluid-phase configurations were generated for each ferrogel.

The solid ferrogel was modeled at zero pressure in an orthorhombic cell by performing independent moves in the box dimensions L_x, L_y, and L_z. The DHSs underwent only orientational moves because real magnetic grains are locked in to the ferrogel matrix. The effects of the gel were represented with an elastic potential

$$U_{el} = \frac{1}{2} L_0^3 G_0 \sum_{\alpha=x,y,z} \left(\frac{L_\alpha}{L_0} - 1 \right)^2, \tag{3}$$

where $L_0 = \langle L \rangle_f$ is the equilibrium cubic box length of the elastic matrix. Simulations of the ferrogel in an arbitrary homogeneous magnetic field $\boldsymbol{H}_g$ were performed according to the Boltzmann distribution,

$$p_g \propto \exp\left[-\beta(U_{DHS} + U_{el} - \mu_0 \boldsymbol{H}_g \cdot \boldsymbol{M})\right], \tag{4}$$

where the subscript "g" refers to simulations in the ferrogel phase. Note that the factors of V^N and $\exp(-\beta PV)$ are now omitted because the only degrees of freedom are the dipole orientations and the box lengths, and the latter are sampled as if the gel is a solid body with embedded interaction sites, undergoing affine thermal fluctuations under zero applied pressure.[1] The elastic modulus of the ferrogel in direction α was determined by measuring fluctuations in the corresponding strain [37],

$$G_\alpha = \frac{k_B T}{\langle V \rangle_g \langle \epsilon_\alpha^2 \rangle_g}, \tag{5}$$

where

$$\epsilon_\alpha = \frac{L_\alpha}{\langle L_\alpha \rangle_g} - 1 \tag{6}$$

and $\langle L_\alpha \rangle_g$ and $\langle V \rangle_g$ are, respectively, the average box lengths and volume of the ferrogel and not those for the parent fluid which may have been prepared under a different applied magnetic field. All ferrogel properties were averaged over at least 20 simulations of 10^6 MC sweeps, each started from an independent particle configuration generated in the fluid phase. It is noted that systematic finite-size errors appear to be insignificant compared to the statistical errors arising from sampling different configurations. Spot checks were made with simulations of $N = 500$ DHSs, and the results were in agreement with those from 250-particle simulations within statistical errors.

[1]To show that Eq. (4) is correct, imagine that the DHS and dipole-field interactions are turned off so that $p_g \propto \exp(-\beta U_{el})$. For a large-enough system in which the fluctuations in L_α are small compared to L_0, the ensemble averages are given in terms of elementary Gaussian integrals and so $\langle L_\alpha \rangle = L_0$ and $G_\alpha = G_0$ (5), which are the correct ensemble averages for the gel containing noninteracting particles.

Three distinct situations have been studied: (i) a ferrogel prepared with no magnetic field applied ($\boldsymbol{H}_f = \boldsymbol{0}$); (ii) a ferrogel prepared with a magnetic field $\boldsymbol{H}_f = (H_x,0,0)$; and (iii) a ferrogel prepared with a magnetic field $\boldsymbol{H}_f = (0,0,H_z)$. In each case, the properties of the ferrogel were measured with a field applied in the x direction, $\boldsymbol{H}_g = (H_x,0,0)$, so that in cases (ii) and (iii) the field is parallel and perpendicular, respectively, to the enhanced positional correlations in the parent fluid phase. With realistic parameters, the anisotropy of the microstructure is not apparent from the simulation snapshots; some snapshots are shown in Fig. 1. The extent of the correlations is discussed in detail in Sec. III.

A. Parameters and reduced units

All simulations were performed in reduced units defined using the DHS diameter σ as the basic unit of length and the thermal energy $k_B T$ as the basic unit of energy. Experimental conditions vary widely, but some characteristic choices are made here to afford some contact with real materials. Real ferrogels are often synthesized with magnetic compositions in the region of 10%–30% by weight. The magnetic component may consist of roughly spherical grains of magnetite (Fe_3O_4) with mean diameters $\sigma \sim 10$ nm [12,23,24]. The mass density of magnetite is 5 g cm^{-3} and by assuming that the polymer gel has a mass density close to 1 g cm^{-3}, the required volume fraction of magnetic grains is $\varphi = \pi\rho\sigma^3/6 \sim 0.01$ – 0.1. *N-P-T* simulations of the fluid phase were carried out with $\beta P\sigma^3 = 0.15$ and 0.25, giving volume fractions of $\varphi \simeq 0.07$ and 0.10, respectively. For magnetite the saturation

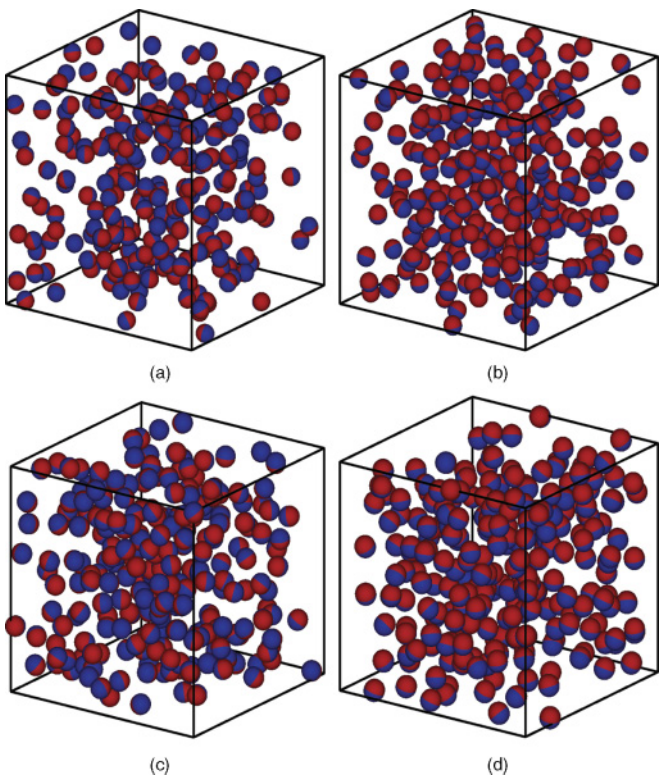

FIG. 1. (Color online) Simulation snapshots of DHS fluids. (a) $\boldsymbol{H}_f^* = \boldsymbol{0}$, $\varphi = 0.064$; (b) $\boldsymbol{H}_f^* = (0,0,5)$, $\varphi = 0.071$; (c) $\boldsymbol{H}_f^* = \boldsymbol{0}$, $\varphi = 0.096$; (d) $\boldsymbol{H}_f^* = (0,0,5)$, $\varphi = 0.106$.

TABLE I. Results for model ferrogels prepared from the fluid phase in a magnetic field $\boldsymbol{H}_\mathrm{f}$. P is the osmotic pressure of the DHSs in the fluid phase, ρ is the concentration of DHSs, and φ is the corresponding volume fraction. M_x is the average magnetization in the field direction. $G_\alpha(0)$ and ΔG_α are the fitting parameters in Eqs. (12) and (13) relating the elastic moduli to the magnetization in the x direction. The figures in brackets are the estimated statistical uncertainties in the final digits.

$\boldsymbol{H}_\mathrm{f}^*$	$\beta P\sigma^3$	$\rho\sigma^3$	φ	$M_x/N\mu$	$\beta G_x(0)\sigma^3$	$\beta\Delta G_x\sigma^3$	$\Delta G_x/G_x(0)$	$\beta G_z(0)\sigma^3$	$\beta\Delta G_z\sigma^3$
0	0.15	0.123	0.064	0.0004(2)	15.88(14)	2.97(30)	0.187(19)	15.52(34)	−0.06(78)
0	0.25	0.183	0.096	−0.0003(2)	20.92(24)	7.76(65)	0.371(31)	20.66(13)	2.01(37)
(5,0,0)	0.15	0.136	0.071	0.81611(8)	20.85(13)	8.33(29)	0.399(14)	15.03(14)	1.07(36)
(5,0,0)	0.25	0.203	0.106	0.82179(7)	27.862(56)	24.00(14)	0.8614(54)	20.78(17)	2.70(43)
(0,0,5)	0.15	0.136	0.071	0.81611(8)	14.90(21)	2.70(46)	0.181(31)	19.692(63)	−1.77(14)
(0,0,5)	0.25	0.203	0.106	0.82179(7)	19.099(51)	8.39(12)	0.4393(64)	25.95(11)	−3.80(24)

magnetization is $M_\mathrm{s} = 4.8 \times 10^5$ A m^{-1} at $T = 293$ K. The reduced dipole moment is defined as $\mu^* = \sqrt{\beta\mu_0\mu^2/4\pi\sigma^3}$ and with $\mu = \pi M_\mathrm{s}\sigma^3/6$, this parameter has a value of 1.25 at room temperature. In this work, a value of $\mu^* = 1$ is used throughout. The reduced magnetic-field strength is defined as $H^* = H\sqrt{4\pi\beta\mu_0\sigma^3}$. A value of $H^* = 1$ corresponds to a real magnetic-field strength of $H = 16$ kA m^{-1} (or $B = 20$ mT); values of H^* in the range 1–10 correspond to the magnetic fields typically applied in experiments. The reduced elastic modulus is defined as $G^* = \beta G\sigma^3$. Typical cross-linked polymer gels have elastic moduli $G_0 \sim 10$–100 kPa, corresponding to reduced elastic moduli $G_0^* \sim 2$ –20. In this work, a value of $G_0^* = 10$ is used throughout.

III. RESULTS

Table I summarizes some basic parameters for the systems considered in this work. For the fluid phases simulated with an applied field, a reduced magnetic-field strength of $H^* = 5$ was found to give a high magnetization $M/N\mu \simeq 0.8$; fluid configurations at this field strength were used for the subsequent ferrogel simulations. For a given osmotic pressure P, the average concentration of DHSs in the fluid phase varies only weakly with applied field. When the elastic gel potential is switched on, the average concentration changed by an insignificant amount; the precise values are reported for each ferrogel in what follows.

A. $\boldsymbol{H}_\mathrm{f}^* = \mathbf{0}$, $\boldsymbol{H}_\mathrm{g}^* = (H_x^*,0,0)$

Figure 2 shows results for model ferrogels at two different concentrations, prepared with no magnetic field applied. In real applications, the deformation of a ferrogel in an applied magnetic field is best characterized with reference to the zero-field dimensions. Relative deformations are therefore defined by

$$\delta(\cdots) = \frac{\langle\cdots\rangle_\mathrm{g}(H_x)}{\langle\cdots\rangle_\mathrm{g}(0)} - 1. \tag{7}$$

$\delta(L_\alpha)$ and $\delta(V)$ are shown in Fig. 2 for each of the model ferrogels as a function of applied field $\boldsymbol{H}_\mathrm{g}^* = (H_x^*,0,0)$. The x dimensions of the system shrink a little due to the alignment and nose-to-tail attraction of the dipoles along the direction of the field, while the transverse dimensions expand due to the corresponding side-by-side parallel repulsions. Nonetheless, these distortions are much less than 1% and are therefore insignificant (as observed in experiments). The variation in the system volume is also insignificant, being on the order of 0.1%. It is therefore safe to make the common assumption that the overall volume is fixed. The concentrations of DHSs therefore

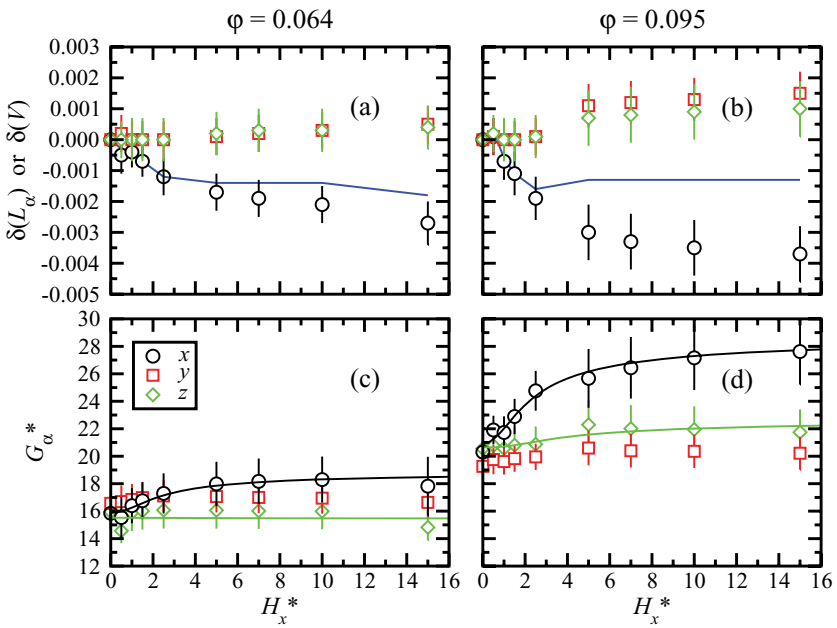

FIG. 2. (Color online) Relative deformations δ (top row) and elastic moduli G_α (bottom row) as functions of the applied magnetic field $\boldsymbol{H}_\mathrm{g}^* = (H_x^*,0,0)$ for model ferrogels prepared with no magnetic field applied and at magnetic volume fractions $\varphi = 0.064$ (left column) and $\varphi = 0.095$ (right column). In (a) and (b) the points are $\delta(L_\alpha)$ ($\alpha = x,y,z$) and the line is $\delta(V)$. In (c) and (d) the points are from simulations and the solid lines are from Eqs. (12) and (13) with $M_x(H_x)$ given by Eq. (10). Properties in the x, y, and z directions are indicated by circles, squares, and diamonds, respectively.

remain roughly constant with applied field, and the average concentrations shown in Fig. 2 apply to each field strength and vary imperceptibly from the fluid-phase concentrations reported in Table I. Snapshots of the DHS configurations are shown in Figs. 1(a) and 1(c).

The elastic moduli G_α are shown in Fig. 2. First, the elastic moduli are seen to increase with increasing DHS concentration due to the influence of the interparticle interactions. Upon the application of a field, the elastic modulus in the field direction (G_x) increases with increasing field strength, while the elastic moduli in the transverse directions (G_y,G_z) remain roughly constant. The increase in G_x is more pronounced at the higher DHS concentration, in good correspondence with what is observed in experiments. To compare further with experiment, a DHS volume fraction of $\varphi = 0.064$ equates to a magnetic loading of about 25 wt%. In this case, G_x^* increases by 13% from 16 to 18; in real units, this corresponds to $G_x = 65$–73 kPa. This enhancement is comparable to that seen in some experiments, but a more detailed comparison is precluded by the large number of variables such as particle-size polydispersity (and its relation to ferromagnetism and intrinsic superparamagnetism), polymer-gel elastic modulus, and range of magnetic-field strengths that differ from study to study.

B. $\boldsymbol{H}_f^* = (5,0,0)$, $\boldsymbol{H}_g^* = (H_x^*,0,0)$

Figure 3 shows results for model ferrogels at two different concentrations, prepared with a magnetic field $\boldsymbol{H}_f^* = (5,0,0)$. As for the zero-field case, the relative deformations $\delta(L_\alpha)$ and $\delta(V)$ are less than 1% and the overall DHS concentration remains almost constant over the whole range of magnetic-field strengths. An applied magnetic field increases the elastic modulus in the field direction, while the elastic moduli in the transverse directions show only very slight increases; these changes are mirrored by the very small but systematic variations in $\delta(L_\alpha)$. In the system with $\varphi = 0.071$ (corresponding to a loading of 28 wt%) G_x^* increases by 33% from 21 to 28 (in real units 85–113 kPa). This increase is greater than that in the $\boldsymbol{H}_f = \boldsymbol{0}$ case discussed previously; this is in qualitative agreement with experiment. Clearly, this has to do with the way the particles are positioned in the matrix.

Figures 1(b) and 1(d) show that there are no clearly defined chainlike clusters. Nonetheless, the dipolar orientations are aligned by an applied field and the particle positions show enhanced nose-to-tail correlations in the field direction. Figure 4 shows a two-dimensional, grayscale plot of the pair correlation function $g(r_\parallel,r_\perp)$, where $r_\parallel$ and $r_\perp$ are the

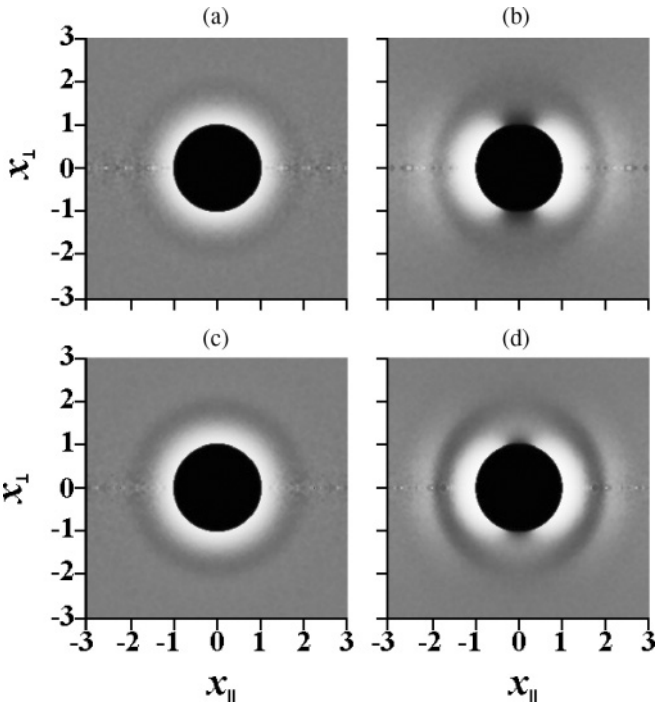

FIG. 4. Grayscale plots of the pair correlation function $g(r_\parallel,r_\perp)$ in DHS fluids; $x = r/\sigma$ is the dimensionless distance. (a) $\boldsymbol{H}_f^* = \boldsymbol{0}$, $\varphi = 0.064$; (b) $\boldsymbol{H}_f^* = (5,0,0)$, $\varphi = 0.071$; (c) $\boldsymbol{H}_f^* = \boldsymbol{0}$, $\varphi = 0.096$; (d) $\boldsymbol{H}_f^* = (5,0,0)$, $\varphi = 0.106$.

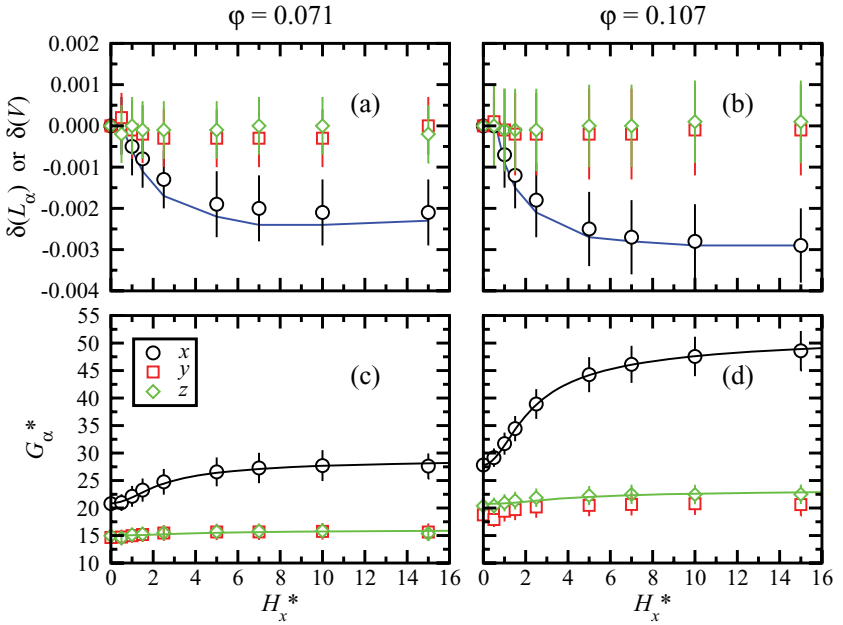

FIG. 3. (Color online) Relative deformations δ (top row) and elastic moduli G_α (bottom row) as functions of the applied magnetic field $\boldsymbol{H}_g^* = (H_x^*,0,0)$ for model ferrogels prepared in a field $\boldsymbol{H}_f^* = (5,0,0)$ and at magnetic volume fractions $\varphi = 0.071$ (left column) and $\varphi = 0.107$ (right column). In (a) and (b) the points are $\delta(L_\alpha)$ ($\alpha = x,y,z$) and the line is $\delta(V)$. In (c) and (d) the points are from simulations and the solid lines are from Eqs. (12) and (13) with $M_x(H_x)$ given by Eq. (10). Properties in the x, y, and z directions are indicated by circles, squares, and diamonds, respectively.

parallel and perpendicular projections, respectively, of the pair separation vector on to the magnetic-field direction. The light regions show that there are enhanced positional correlations in the field direction. Consequently, when a field is applied to the ferrogel in the same direction, the interparticle forces are enhanced. A thorough theoretical and simulation analysis of anisotropic correlations in DHS fluids is under way [38].

Interestingly, there is already a degree of anisotropy in the elastic moduli in zero field: the material is stiffer in the x direction than in the y and z directions. This is also due to the enhanced positional correlations in the x direction; even in zero field, the DHSs are still close to contact and interacting with each other strongly through both the hard-core and the dipolar forces. The particles are separated further from one another in the y and the z directions, however, and this leads to a relative softening of the material in those directions. The zero-field anisotropy observed here is in qualitative agreement with what is seen experimentally [12,23,24,27].

C. $\boldsymbol{H}_{\rm f}^* = (0,0,5)$, $\boldsymbol{H}_{\rm g}^* = (H_x^*,0,0)$

The final situation to be studied is when the field applied to the fluid phase is perpendicular to the field applied to the resulting ferrogel. Figure 5 shows the results. Once again, the relative deformations of the ferrogel in an applied field are rather small, being less than 1%. In zero field, the elastic moduli show anisotropies opposite to those in the previous section: The elastic modulus in the direction of $\boldsymbol{H}_{\rm f}$ (now the z direction) is greater than those in the other two directions; this is in good correspondence with experiment. As before, this is due to the presence of enhanced positional correlations in the field direction between particles close to contact. An applied magnetic field increases the elastic modulus in the field direction (x) and decreases that in the z direction. The particle positions are correlated in the z direction but the dipoles are oriented along the x axis (side-by-side parallel), which means that the dipoles repel along the z direction; this manifests itself in a very slight increase in $\delta(L_z)$ and a reduction in the elastic modulus. Although no chainlike clusters are apparent in the simulation configurations, enhanced correlations in the field direction are certainly there as already shown in Fig. 4. For the ferrogel with $\varphi = 0.071$ (corresponding to a loading of 28 wt%) G_x^* increases by 13% from 15 to 17 (in real units 61–69 kPa); this change is in good agreement with that typically seen in experiments. The elastic modulus and deformation in the y direction show almost no changes.

D. The relationships between the elastic moduli, the magnetization, and the field

Figures 2, 3, and 5 show the variations of G_α with magnetic-field strength H_x. Now attention is turned to the detailed variation of G_x (along the field direction). In earlier work, Varga *et al.* noted that at small H_x, $G_x(H_x) - G_x(0) \propto H_x^2$, while at large H_x, $G_x(\infty) - G_x(H_x) \propto 1/H_x^2$ [12,27]. On this basis, they proposed a fitting function equivalent to

$$G_x(H) = G_x(0) + \Delta G_x \left(\frac{H_x^2}{a_H + H_x^2} \right), \qquad (8)$$

where a_H is a material parameter. Equation (8) gives excellent fits to experimental data, but it is a heuristic relationship and it would be desirable to obtain a more physically transparent form. To this end, note that at small H_x, the magnetization curve $M_x(H_x) \approx \chi H_x$, where χ is the initial magnetic susceptibility. This suggests that G_x may have a very simple dependence on the square of the corresponding magnetization M_x^2; the magnetization curve will be considered first, and then the dependence of G_x on M_x will be revealed. At large H_x, the magnetization reaches saturation as $M_x(H_x) \approx N\mu - N/\beta\mu_0 H_x$ because the field-dipole interaction dominates and so the magnetization curve reduces to the appropriate limit of the single-particle, Langevin result:

$$M_x^{\rm L}(H_x) = N\mu \left[\coth(\beta\mu_0\mu H_x) - \frac{1}{\beta\mu_0\mu H_x} \right]. \qquad (9)$$

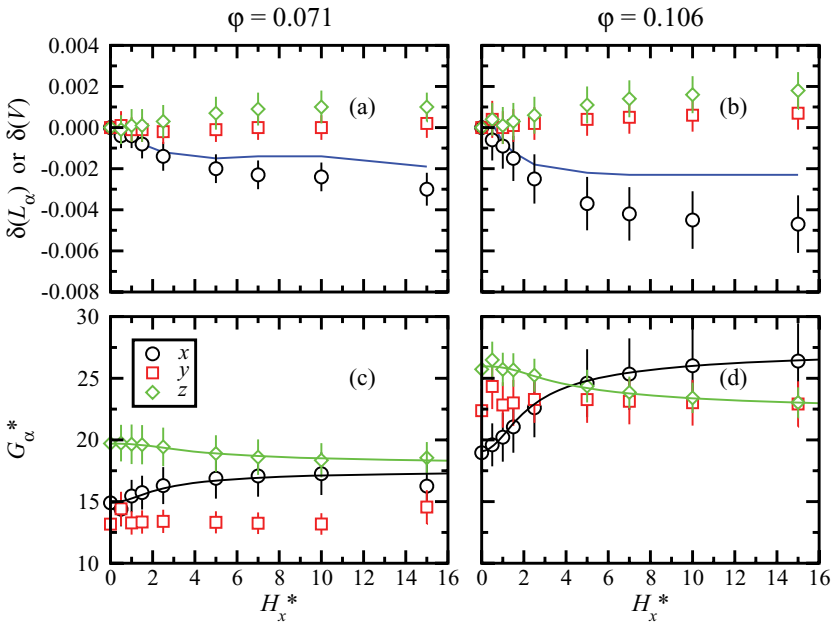

FIG. 5. (Color online) Relative deformations δ (top row) and elastic moduli G_α (bottom row) as functions of the applied magnetic field $\boldsymbol{H}_{\rm g}^* = (H_x^*,0,0)$ for model ferrogels prepared in a field $\boldsymbol{H}_{\rm f}^* = (0,0,5)$ and at magnetic volume fractions $\varphi = 0.071$ (left column) and $\varphi = 0.106$ (right column). In (a) and (b) the points are $\delta(L_\alpha)$ ($\alpha = x,y,z$) and the line is $\delta(V)$. In (c) and (d) the points are from simulations and the solid lines are from Eqs. (12) and (13) with $M_x(H_x)$ given by Eq. (10). Properties in the x, y, and z directions are indicated by circles, squares, and diamonds, respectively.

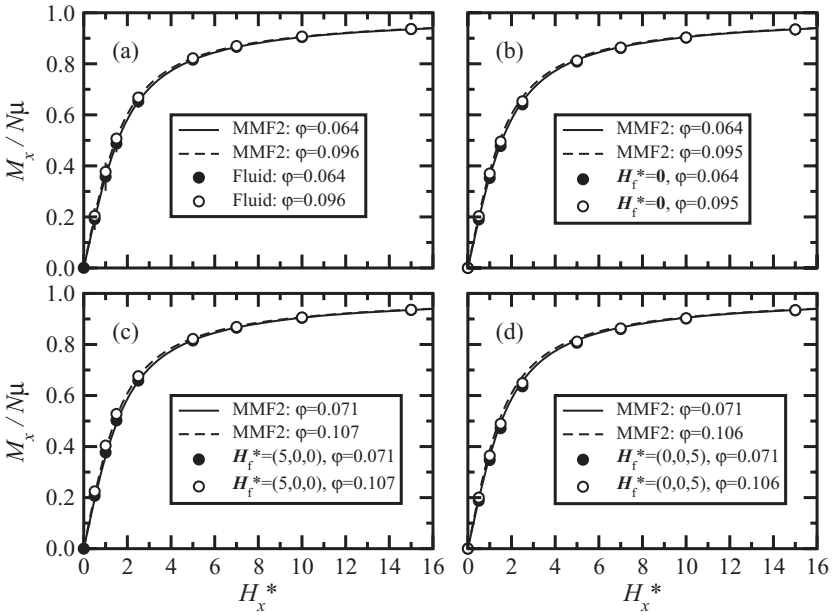

FIG. 6. Magnetization curves for ferrofluids and ferrogels (points) with the predictions of modified mean-field theory for the fluid phase (lines). (a) Fluids. (b) Ferrogels prepared with no magnetic field applied. (c) Ferrogels prepared in a field $\boldsymbol{H}_{\mathrm{f}}^{*} = (5,0,0)$. (d) Ferrogels prepared in a field $\boldsymbol{H}_{\mathrm{f}}^{*} = (0,0,5)$. The volume fractions φ of DHSs are indicated in the legend.

Figure 6 shows the magnetization curves for two DHS fluids and all six of the model ferrogels studied in this work. There is very little dependence on the DHS concentration and the preparation conditions. (In all cases, M_y and M_z are zero within the statistical uncertainties.) Theoretical magnetization curves for DHS *fluids* are shown for comparison. According to the modified mean-field theory of Ivanov and Kuznetsova [32], the fluid magnetization curve is

$$M_x(H_x) = M_x^{\mathrm{L}}\left(H_x^{\mathrm{eff}}\right), \tag{10}$$

where the effective field H_x^{eff} is given by

$$H_x^{\mathrm{eff}} = H_x + \frac{4\pi}{3}\frac{M_x^{\mathrm{L}}(H_x)}{V} + \frac{(4\pi)^2}{144}\frac{M_x^{\mathrm{L}}(H_x)}{V^2}\frac{\mathrm{d}M_x^{\mathrm{L}}}{\mathrm{d}H_x}. \tag{11}$$

The modification of the field accounts for dipole-dipole interactions in a systematic perturbation-theory expansion in terms of ρ and βU_{DHS} [32]. Equation (10) has been shown to give an excellent account of the magnetization curves in real and simulated ferrofluids, and the corresponding predictions for the magnetic susceptibility are also highly accurate [28,29,32,33]. This is reconfirmed for DHS fluids in Fig. 6(a). Figures 6(b)–6(d) show that Eq. (10) also gives adequate descriptions for the ferrogels.

Figure 7 shows the elastic modulus G_x plotted against M_x^2 for all six ferrogels studied in this work. As anticipated, the results can be fitted accurately using the simple relationship

$$G_x(M_x) = G_x(0) + \Delta G_x \left(\frac{M_x}{N\mu}\right)^2, \tag{12}$$

where $0 \leqslant M_x/N\mu \leqslant 1$ is a dimensionless, fractional measure of the magnetization. On symmetry grounds, $G_x(M_x)$ must be an even function of M_x and the high quality of the fits suggests that terms higher in order than M_x^2 are not required. The fit parameters $G_x(0)$ and ΔG_x are given in Table I. Figure 7 illustrates succinctly how the degree of enhancement in G_x depends on the DHS concentration and the preparation conditions, as discussed in Secs. III A–III C. A convenient measure for the maximum possible enhancement in G_x is the ratio $\Delta G_x/G_x(0)$; these values are included in Table I and confirm that, as seen in experiments, the greatest enhancement in elastic modulus is achieved when $\boldsymbol{H}_{\mathrm{f}}$ and $\boldsymbol{H}_{\mathrm{g}}$ are parallel.

Equations (10) and (12) can be combined to yield the relationship between G_x and H_x. The resulting curves are shown in Figs. 2, 3, and 5. In all cases the agreement with simulation is essentially perfect. A better representation for the magnetization curve may be sought [34], but Eq. (10) is clearly adequate for the current purposes.

In the ferrogels prepared with $\boldsymbol{H}_{\mathrm{f}}^{*} = \boldsymbol{0}$ and $\boldsymbol{H}_{\mathrm{f}}^{*} = (5,0,0)$, G_y and G_z show only very weak dependencies on the applied field. In the $\boldsymbol{H}_{\mathrm{f}}^{*} = (0,0,5)$ case, however, G_z exhibits an interesting dependence on H_x. By analogy with Eq. (12), a

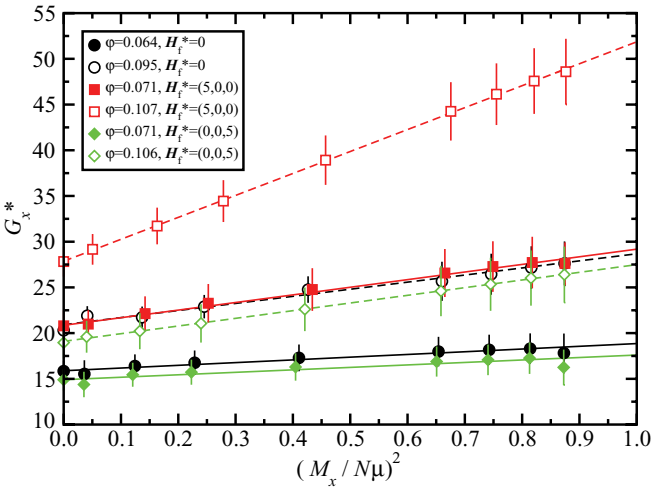

FIG. 7. (Color online) Ferrogel elastic modulus G_x as a function of the square of the magnetization M_x^2 (points) with the fits from Eq. (12) (lines). The magnetic fields and volume fractions φ of DHSs are indicated in the legend.

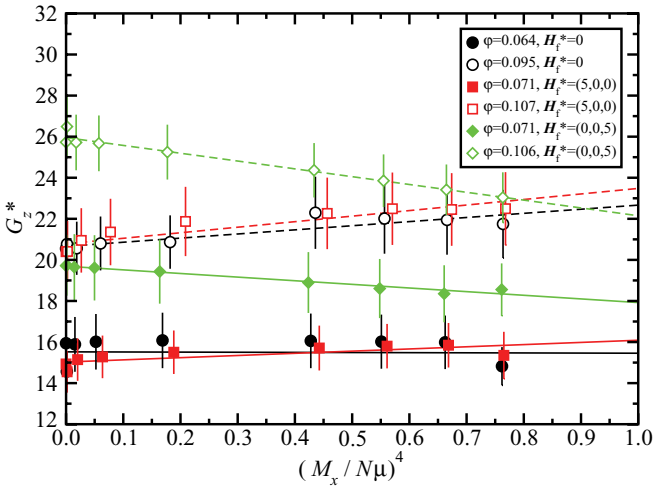

FIG. 8. (Color online) Ferrogel elastic modulus G_z as a function of the fourth power of the magnetization M_x^4 (points) with the fits from Eq. (13) (lines). The magnetic fields and volume fractions φ of DHSs are indicated in the legend.

simple relationship between G_z and M_x is sought. It turns out that, heuristically, the best expression for fitting is

$$G_z(M_x) = G_z(0) + \Delta G_z \left(\frac{M_x}{N\mu} \right)^4 . \tag{13}$$

Figure 8 shows G_z plotted against M_x^4 for all six ferrogels studied in this work. Excellent fits are obtained, although the variations in G_z for the $\boldsymbol{H}_f^* = \mathbf{0}$ and $\boldsymbol{H}_f^* = (5,0,0)$ cases are small; the fitting parameters are given in Table I.

When supplemented by the magnetization curve from Eq. (10), Eq. (13) furnishes an expression for G_z in terms of H_x. The resulting curves are shown in Figs. 2, 3, and 5. Once again, the agreement with simulation is essentially perfect.

Finally, the anisotropy of a ferrogel can be characterized by a simple parameter such as

$$A_{xz} = \frac{G_x - G_z}{G_x + G_z}, \tag{14}$$

where the x and z components are selected because they show the greatest variations. Figure 9 shows A_{xz} for all six ferrogels. In the $\boldsymbol{H}_f^* = \mathbf{0}$ case, the zero-field anisotropy is essentially zero within the statistical uncertainties. Applying a field increases the anisotropy, with the effect being more highly pronounced at higher concentration. In the $\boldsymbol{H}_f^* = (5,0,0)$ case, the zero-field anisotropy and high-field asymptote are greater than those for the $\boldsymbol{H}_f^* = \mathbf{0}$ case. The zero-field anisotropy in the $\boldsymbol{H}_f^* = (0,0,5)$ case is negative because of the stiffening in the z direction, as discussed in Sec. III C. With $\boldsymbol{H}_f^* = (0,0,5)$ and $\varphi = 0.106$ it is possible to tune the magnetic field ($H_x^* \simeq 5$) so that the elastic moduli in the x and z directions are equal. Of the three cases, the greatest anisotropy is achieved with $\boldsymbol{H}_f^* = (5,0,0)$. Equations (12), (13), and (10) can be substituted in to Eq. (14) to describe the dependence of the anisotropy on the applied field. Figure 9 shows the resulting curves, which are in excellent agreement with the simulation data.

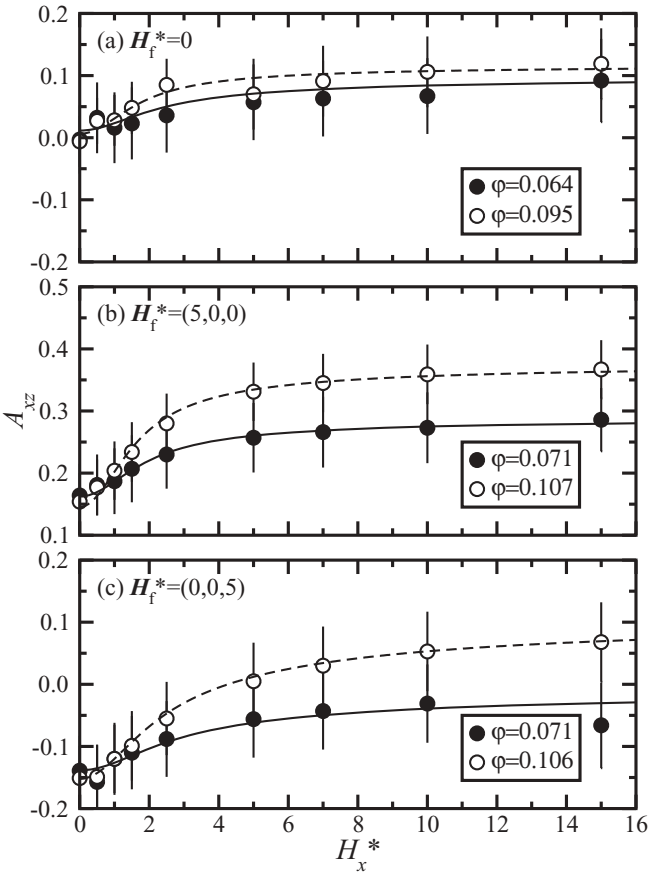

FIG. 9. Anisotropy $A_{xz} = (G_x - G_z)/(G_x + G_z)$ of the elastic moduli in the x and z directions. (a) Ferrogels prepared with no magnetic field applied. (b) Ferrogels prepared in a field $\boldsymbol{H}_f^* = (5,0,0)$. (c) Ferrogels prepared in a field $\boldsymbol{H}_f^* = (0,0,5)$. The volume fractions φ of DHSs are indicated in the legend. The points are from simulations and the lines are from a combination of Eqs. (12) and (13) with $M_x(H_x)$ given by Eq. (10).

IV. CONCLUSIONS

A simple microscopic model of ferrogels has been described and its properties have been determined using MC simulations. The model represents the material as a dispersion of DHSs trapped in an elastic matrix. In this preliminary study, a portion of ferrogel was restricted to be orthorhombic and only allowed to undergo affine deformations. Despite the simplicity of the model, it captures much of the phenomenology from experimental studies. Specifically, the elastic moduli of ferrogels can be tuned by applying uniform magnetic fields during the gel-formation stage; the field gives rise to a subtle enhancement of positional correlations between magnetic grains and a pronounced anisotropy to the material properties. A very significant enhancement of the elastic modulus can then be observed if the ferrogel is then placed in a parallel uniform field; less pronounced effects occur with other arrangements of fields during and after the synthesis stage. It has been demonstrated using MC simulations that the model ferrogel mimics experimental trends quite reliably, while providing specific insights on the microscopic arrangements of the magnetic grains. In addition to these insights, the simulation results suggest a particularly simple relationship between the

elastic moduli and the magnetization; when supplemented by a magnetization curve, this relationship leads to the dependence of the elastic moduli on the magnetic-field strength, which is normally the property measured directly in experiments.

A number of improvements to the model can be envisaged. An extension of the model to the case of paramagnetic particles should be attempted. Although ferrogels are often made with nanometer-sized ferromagnetic or intrinsically superparamagnetic particles, some more recent applications may require materials made from larger particles that do not possess single magnetic domains. Another feature of real ferrogels is the polydispersity of the magnetic-grain sizes and dipole moments. In other contexts, magnetic polydispersity has been shown to have quite significant effects [28,29]. The model might also be extended to take in to account shear deformations and nonaffine deformations; an explicit model of the cross-linked polymer gel component would help accommodate local nonaffine displacements of the magnetic grains within a simulation box of triclinic geometry. Despite the simplicity of the current model, however, the correspondence with experiment is quite good. As a proof of principle, it is hoped that this study will stimulate further links to be made between the microscopic and macroscopic properties of ferrogels.

ACKNOWLEDGMENTS

D.S.W. acknowledges support from the School of Chemistry at the University of Edinburgh.

[1] M. Zrínyi, L. Barsi, and A. Büki, J. Chem. Phys. **104**, 8750 (1996).
[2] M. Zrínyi, L. Barsi, D. Szabó, and H.-G. Kilian, J. Chem. Phys. **106**, 5685 (1997).
[3] M. Zrínyi, Colloid Polym. Sci. **278**, 98 (2000).
[4] R. E. Rosensweig, *Ferrohydrodynamics* (Dover, New York, 1998).
[5] K. Zimmermann, V. A. Naletova, I. Zeidis, V. Böhm, and E. Kolev, J. Phys. Condens. Matter **18**, S2973 (2006).
[6] K. Zimmermann, V. A. Naletova, I. Zeidis, V. A. Turkov, E. Kolev, M. V. Lukashevich, and G. V. Stepanov, J. Magn. Magn. Mater. **311**, 450 (2007).
[7] M. Babincová, D. Leszczynska, P. Sourivong, P. Čičmanec, and P. Babinec, J. Magn. Magn. Mater. **225**, 109 (2001).
[8] L. L. Lao and R. V. Ramanujan, J. Mat. Sci. **15**, 1061 (2004).
[9] T.-Y. Liu, S.-H. Hu, T.-Y. Liu, D.-M. Liu, and S.-Y. Chen, Langmuir **22**, 5974 (2006).
[10] L. Barsi and M. Zrínyi, ACH Models Chem. **135**, 241 (1998).
[11] R. V. Ramanujan and L. L. Lao, Smart Mater. Struct. **15**, 952 (2006).
[12] G. Filipcsei, I. Csetneki, A. Szilágyi, and M. Zrínyi, Adv. Polym. Sci. **206**, 137 (2007).
[13] A. T. Ngo, J. Richardi, and M.-P. Pileni, Nano Lett. **8**, 2485 (2008).
[14] L. Pauchard, F. Elias, P. Boltenhagen, A. Cebers, and J. C. Bacri, Phys. Rev. E **77**, 021402 (2008).
[15] Yu. L. Raikher and O. V. Stolbov, J. Magn. Magn. Mater. **258-259**, 477 (2003).
[16] Yu. L. Raikher and O. V. Stolbov, J. Appl. Mech. Tech. Phys. **46**, 434 (2005).
[17] Yu. L. Raikher and O. V. Stolbov, J. Magn. Magn. Mater. **289**, 62 (2005).
[18] O. V. Stolbov and Yu. L. Raikher, J. Magn. Magn. Mater. **300**, e199 (2006).
[19] C. Gollwitzer, A. Turanov, M. Krekhova, G. Lattermann, I. Rehberg, and R. Richter, J. Chem. Phys. **128**, 164709 (2008).
[20] Yu. L. Raikher and O. V. Stolbov, J. Phys. Condens. Matter **20**, 204126 (2008).
[21] K. Morozov, M. Shliomis, and H. Yamaguchi, Phys. Rev. E **79**, 040801(R) (2009).
[22] L. V. Nikitin, G. V. Stepanov, L. S. Mironova, and A. I. Gorbunov, J. Magn. Magn. Mater. **272-276**, 2072 (2004).
[23] Z. Varga, G. Filipcsei, A. Szilágyi, and M. Zrínyi, Macromol. Symp. **227**, 123 (2005).
[24] Z. Varga, G. Filipcsei, and M. Zrínyi, Polymer **46**, 7779 (2005).
[25] L. V. Nikitin, G. V. Stepanov, L. S. Mironova, and A. N. Samus, J. Magn. Magn. Mater. **258-259**, 468 (2006).
[26] L. V. Nikitin, D. G. Korolev, G. V. Stepanov, and L. S. Mironova, J. Magn. Magn. Mater. **300**, e234 (2006).
[27] Z. Varga, G. Filipcsei, and M. Zrínyi, Polymer **47**, 227 (2006).
[28] A. O. Ivanov, S. S. Kantorovich, E. N. Reznikov, C. Holm, A. F. Pshenichnikov, A. V. Lebedev, A. Chremos, and P. J. Camp, Phys. Rev. E **75**, 061405 (2007).
[29] A. O. Ivanov, S. S. Kantorovich, E. N. Reznikov, C. Holm, A. F. Pshenichnikov, A. V. Lebedev, A. Chremos, and P. J. Camp, Magnetohydrodynamics **43**, 393 (2007).
[30] M. R. Jolly, J. D. Carlson, B. C. Munoz, and T. J. Bullions, J. Intell. Mater. Syst. **7**, 613 (1996).
[31] M. R. Dudek, B. Grabiec, and K. W. Wojciechowski, Rev. Adv. Mater. Sci. **14**, 167 (2007).
[32] A. O. Ivanov and O. B. Kuznetsova, Phys. Rev. E **64**, 041405 (2001).
[33] A. O. Ivanov and O. B. Kuznetsova, Colloid J. **68**, 430 (2006).
[34] E. Jarkova, H. Pleiner, H.-W. Müller, and H. R. Brand, Phys. Rev. E **68**, 041706 (2003).
[35] M. P. Allen and D. J. Tildesley, *Computer Simulation of Liquids* (Clarendon Press, Oxford, 1987).
[36] D. Frenkel and B. Smit, *Understanding Molecular Simulation: From Algorithms to Applications*, 2nd ed. (Academic Press, San Diego, 2001).
[37] M. Parrinello and A. Rahman, J. Chem. Phys. **76**, 2662 (1982).
[38] E. A. Elfimova, A. O. Ivanov, and P. J. Camp (unpublished).